Journal of Alloys and Compounds 509 (2011) 2672–2678

Contents lists available at ScienceDirect

Journal of Alloys and Compounds

journal homepage: www.elsevier.com/locate/jallcom

Efficient dual functionality of highly porous nanocomposites based on TiO_2 and noble metal particles

L. Baia[a,*], L. Diamandescu[b], L. Barbu-Tudoran[c], A. Peter[d], G. Melinte[a], V. Danciu[d], M. Baia[a]

[a] Faculty of Physics, Babes-Bolyai University, M. Kogalniceanu 1, 400084 Cluj-Napoca, Romania
[b] National Institute of Materials Physics, P.O. Box MG-7, 77125 Bucharest, Romania
[c] Faculty of Biology & Geology, Babes-Bolyai University, Clinicilor 5-7, 400006 Cluj-Napoca, Romania
[d] Faculty of Chemistry and Chemical Engineering, Babes-Bolyai University, Arany Janos 11, 400028 Cluj-Napoca, Romania

ARTICLE INFO

Article history:
Received 1 September 2010
Received in revised form
10 November 2010
Accepted 20 November 2010
Available online 1 December 2010

Keywords:
Photocatalysis
SERS sensor
Porous composites
TiO_2 aerogel
Noble metal particles

ABSTRACT

Porous nanocomposites based on TiO_2 aerogels and Au and, respectively, Ag particles were synthesized and their dual functionality to decontaminate water, *via* photocatalysis, and to detect low concentrations of pollutants from water, *via* SERS technique, was evaluated using model pollutants. The apparent photodegradation rate constants of a standard pollutant molecule revealed a considerable improvement of the composites photocatalytic performances (even better than one order of magnitude) in comparison with the commercial product Degussa P25. The essential role of the contact between TiO_2 and Au nanoparticles was demonstrated and the potential of all synthesized porous composites for photocatalytic experiments with visible light was pointed out. The lowest concentrations of contaminants adsorbed on the noble metal particles detectable by SERS were found to depend on the composite and pollutant species type and were determined to be between 10^{-3} and 5×10^{-6} M, and 10^{-8} and 10^{-10} M for off and under resonant excitation, respectively. The morphological (BET, pore size distribution, TEM) and structural (Raman, XRD, diffuse reflectance) particularities of the obtained porous composites were also discussed.

1. Introduction

Nowadays, the development of efficient photocatalysts has become a necessity due to the increased environmental contamination. With the purpose of exploiting this idea many studies performed during the last decades revealed that TiO_2, in various compositional combinations, is one of the most promising materials for photocatalytic applications because it possesses the fundamental characteristics of an ideal photocatalyst: inexpensive, non-toxic, highly photoactive and photostable [1–3]. Its photocatalytic performances can be improved by retarding the electron–hole recombination process that is in direct competition with space–charge separation of the electron and the hole by loading of electron accepting species on its surface. Particularly, the loading of noble metals accelerates the photoexcited electrons transport to the outer system increasing thus the photonic efficiency [4], and leading to an enhancement of the photocatalytic activity [5–7]. On the other hand, the efficient use of solar energy for photocatalysts activation is an important target of the modern science and engineering with a huge impact on technological applications [8]. An extensive literature has already described the doping or loading procedure of TiO_2 with noble metal nanoparticles that directly influences the intrinsic properties of TiO_2 and extends its photoresponse into the visible domain [7,9–19]. In the particular case of TiO_2–Au nanocomposites, a key factor that positively influences the electronic properties is the size of the precious metal particle [14]. For example, Bamwenda et al. [20] shown that 3-nm gold particles supported on titania optimize the effectiveness of CO catalytic oxidation. The existence of a high surface area inside highly porous TiO_2 based nanoarchitectures should also enhances the materials photocatalytic performances [21,22].

TiO_2 aerogels are unique among solid materials with a low density, large open pores, and a high inner surface area that results in interesting physical and chemical properties [21]. The designing of a porous structure based on TiO_2 aerogel and noble metal nanoparticles was found to generate a further improvement of the photocatalytic performances. In this respect, a relevant example is represented by the TiO_2–Au composite aerogels that were found to play an important role to the CO oxidation process [13].

Nanotechnology is currently dedicated to the development of novel materials able to satisfy specific requirements in terms of structural and functional performances, the main trends and breakthroughs being directed towards designing multifunctional structures. Taking into consideration the great potential of TiO_2

* Corresponding author. Fax: +40 264 591906.
E-mail address: lucian.baia@phys.ubbcluj.ro (L. Baia).

0925-8388/$ – see front matter © 2010 Elsevier B.V. All rights reserved.
doi:10.1016/j.jallcom.2010.11.154

for pollutants' photocatalytic destruction, one can infer that the development of titanium dioxide based materials able to take the additional advantage of detecting trace quantities of contaminants by surface-enhanced Raman scattering (SERS) is a challenge. SERS technique is recognized as one of the most sensitive spectroscopic tools available for the detection of a wide range of adsorbed molecules in ultrasensitive limits [23,24], sometimes, down to the single molecule detection limit [25]. The benefit of the Raman enhancement has been already taken into consideration by researchers, who used various systems such as metal colloids (gold and silver), gold–metal island films, silver colloid sol–gel films or other substrates based on silver–polydimethylsiloxane nanocomposites or ultrathin TiO_2 deposited on Ag island films [26–29] for pollutants detection. SERS technique has also been applied to trace analysis of a variety of pollutants in aquatic environments, even in extreme experimental conditions [30]. In our previous work [31], we prepared porous nanoarchitectures based on TiO_2 aerogel and Au colloidal particles and tested their capability to detect by SERS contaminant species adsorbed from an aqueous solution on metallic nanoparticles surface. The composites detection efficiency was established using thioacetamide, crystal violet and rhodamine 6 G as test molecules and, the lowest detectable concentrations were found to be around 10^{-2} M for thioacetamide and in the range between 10^{-5} and 10^{-7} M for dye molecules, off and under resonant excitation, respectively.

Encouraged by the environment friendly character of TiO_2 and the well-known affinity of a large variety of molecules to bind to the noble metal nanoparticles surface we report, in the present work, about the preparation of a new type of highly porous composites based on TiO_2 and Au and, respectively, Ag particles by a different chemical procedure as previously reported [31]. The samples were analyzed from a morphological and structural point of view and, their both capacities to decontaminate water *via* photocatalysis and to detect minute concentrations of pollutants from water *via* SERS technique were evaluated.

2. Experimental

2.1. Materials

Gold and silver colloidal suspensions were prepared according to the procedures reported in the literature [32,33] and were used as obtained. The gold colloidal suspension was prepared as follows [32]: 100 ml of 10^{-3} M $HAuCl_4{\cdot}3H_2O$ was brought to a boil with vigorous stirring on a magnetic stirring hot plate. 10 ml of 38.8 mM $Na_3C_3H_5O(COO)_3{\cdot}2H_2O$ was added to the solution all at once under vigorous stirring. The yellow solution turned clear, dark blue and then a deep red-burgundy color within a few minutes. Stirring and boiling were continued for 15 min after the burgundy color was observed. The solution was removed from heat and kept stirring until it became cold and then the volume was adjusted to 100 ml by adding water.

The silver colloidal suspension was prepared as follows [33]: 100 ml of 5×10^{-3} M $AgNO_3$ was heated to boiling under continuous stirring. 90 ml of 2×10^{-3} M $NaBH_4$ was added dropwise under vigorous stirring. The boiling and stirring of the reaction mixture were continued for another 60 min. Colloidal solutions were stored in clean brown glass bottles until used.

TiO_2 gels were prepared with the acid-catalyzed sol–gel method using titanium isopropoxide (TIP), HNO_3, EtOH and H_2O with the 1/0.08/21/3.675 molar ratios. The gels were allowed to age for three weeks and then immersed into the colloidal suspension for three days. Before supercritical drying with liquid CO_2 (T = 313 K and p = 95.23 atm) the gels impregnated with colloidal nanoparticles were successively washed with excess of fresh EtOH. The obtained composites were porous monoliths with dimensions of a few millimeters and are further denoted with **A** – composites with Au, and **B** – composites with Ag. The color of composites **A** was light-pink, while that of the composites **B** was yellowish-gray.

2.2. Methods

The photocatalytic activity of the composites was established from the degradation rate of salicylic acid that was used as standard pollutant molecule as elsewhere reported [34]. The decrease in time of the salicylic acid concentration (the intensity of the band located at 295 nm) was monitored using a Jasco V-530 UV–vis spectrophotometer ($C_0 = 5 \times 10^{-4}$ M for all investigated samples) (see Fig. 1). The composites immersed in salicylic acid solution were irradiated with a medium pressure Hg HBO OSRAM lamp (500 W). The most intense emission band of the Hg lamp used is located at 365 nm (100% magnitude). The other intense bands are situated around 436 nm (~70%), 312 nm (~50%), 405 nm (~45%), 546 nm (~40%), 577, 302 and 304 nm (~30%). The working temperature was of 20–22 °C and the solution pH was of 5.3. The photodegradation experiments with visible light were performed by filtering out the UV radiation (<400 nm) originating from the Hg lamp.

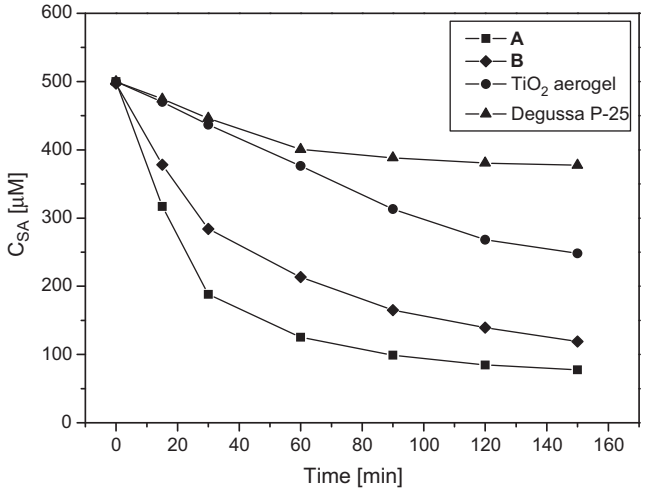

Fig. 1. Evolution of the salicylic acid photodegradation as a function of time in the presence of composites **A** and **B**, TiO_2 aerogel and Degussa P-25 as indicated.

For the photodegradation experiments a quartz cell (12 mm × 12 mm × 65 mm) and an amount of powder of 0.05 g/6 ml widely dispersed on the entire surface of the cell window were used. The radiation was focused on the cell bottom in such a way that the beam diameter was of 10 mm. The distance between the lamp and the cell was of approximately 10 cm. In order to ensure a higher efficiency of the interaction process, i.e. between the radiation and the powder, no stirring was applied. Before visible irradiation as well as before UV–vis measurements, the cell with the sample was kept in dark for 15 min in order to achieve the equilibrium of the adsorption–desorption process. The salicylic acid adsorption on the aerogels surface is indicated by a bright yellow color of their surface (the solution is colourless) originating from the formation of surface charge-transfer complexes [35,36]. Under illumination, the yellow color changes gradually to dark brown, indicating the oxidation of the organic material on the porous composite surfaces. The photodecomposition reaction follows pseudo-first order kinetics and consequently, the apparent rate constant was calculated by plotting $\ln(C_0/C)$ *vs* time. The slope of the plot given by the linear fit represents the apparent rate constant. Throughout the photodecomposition process no shift of the salicylic acid band located at 297 nm was observed.

Elemental analyses were performed with an inductively coupled plasma-mass spectroscope (ICP-MS). The surface area and the pore size distribution of the synthesized samples were determined using a Sorptomatic 1990 (Thermo electron Corp.) equipment and N_2 adsorption.

The phase content and the particle dimensions were determined using a DRON X-ray powder diffractometer linked to a data acquisition and processing facility; CuK_α radiation (λ = 1.540598 Å) and a graphite monochromator were used.

A Jeol JEM 1010 TEM operating at an accelerating voltage of 100 kV and equipped with a MegaViewIII CCD camera was employed to obtain the images. The samples were sonicated for 15 min and then deposited on Cu grids with carbon film evaporated on freshly cleaved mica.

The band gap energy of the composites was calculated from their diffuse reflectance spectra that were recorded by employing a Perkin Elmer Lambda 45 spectrophotometer in the wavelength range of 800–200 nm, with 0.5 nm step at a scan speed of 60 nm/s. Reflectance was converted by the instrument software to $F(R)$ values according to the Kubelka–Munk theory. The band gap was obtained from the plot of $[F(R){\cdot}E]^{1/2}$ versus energy of the exciting light (E) assuming that the investigated porous samples are indirect crystalline semiconductors.

A Nd–YAG laser (λ = 1064 nm) was employed for the recording of Raman spectra of the composites and pollutant molecules. The FT-Raman spectra were recorded using a Bruker Equinox 55 spectrometer with an integrated FRA 106 Raman module, a radiation with a power of 30 mW, incident on sample, and a spectral resolution of 2 cm^{-1}. Prior to perform the SERS measurements, the composites were kept 2–3 min into aqueous solutions of contaminants of various concentrations. SERS spectra were recorded with a Witec confocal Raman system CRM 200 equipped with a 100×/0.8 microscope objective and a 300 lines/mm grating. In the recording of the spectra the 532 and 633 nm laser lines with a power of 3 mW and a spectral resolution around 7 cm^{-1} were employed. In order to ensure the measurements reproducibility SERS spectra were collected from different points located on the composites surface and inside the samples. The measurement time of a SERS spectrum varied from 10to 40 s.

Table 1
BET surface areas, salicylic acid photodegradation rates and TiO_2 and Au/Ag particles size domain.

Sample type	S_{BET} [$m^2\ g^{-1}$]	k_{app} [$\times 10^3\ min^{-1}$]			TiO_2 and Au/Ag particles size [nm]	
		UV–vis	Vis[a]	Vis[b]	TiO_2	Au/Ag
A (TiO_2 aerogel-Au) (0.45Au wt%)	354	31.35	3.9	27.3	5–15	10–24
B (TiO_2 aerogel-Ag) (0.4 Ag wt%)	443	13.30	3.8	26.6	5–15	10–24
TiO_2 aerogel	593	5.75	–	–	10–15	–
Degussa P-25	50	2.50	–	–	~20–anatase~30–rutile	–

[a] The measured photodegradation rate constants after exposure to visible light.
[b] The photodegradation rate constants determined when the incident radiation was exclusively visible light was multiplied by a factor representing the ratio between the incident photon flux for the used UV–vis and the visible radiation.

3. Results and discussion

The main compositional, morphological, structural and photocatalytic data of the synthesized composites derived from elemental analysis, BET, XRD, TEM and UV–vis monitoring of the photodegradation process of salicylic acid are displayed in Table 1. One should note that the values from Table 1 related to Degussa P-25, including the photocatalytic activity, have been obtained in our laboratory and, are specified only for comparison purpose. Moreover, the investigations performed on unloaded TiO_2 aerogel are aimed to reveal how the noble metal nanoparticles influence the photocatalytic performances of the porous composites. To monitor more precisely the evolution of the photocatalytic process, the contaminant photolytic degradation, caused by lower wavelength radiation (UVA and UVB), was evaluated in the catalyst absence. It was found that 5% from pollutant molecules are photolytically destroyed. This result has been taken into consideration in the photocatalytic experiments further performed, all obtained data being accordingly corrected. Thus, the apparent rate constants given in Table 1 do no contain any influence of the photolysis process.

The highest apparent photodegradation rate constant of the standard pollutant was surprisingly obtained for the sample **A**, which has the smallest BET surface area (see Table 1). Besides the decrease of the BET surface area, the presence of noble metal nanoparticles inside the porous TiO_2 network leads to the reduction in pore diameter, as can be seen in Fig. 2. The composite **A**, that pores size distribution is bimodal, has mesopores with average pore diameters of 3.8 and 6 nm, while the composite **B** and TiO_2 aerogel possess average pore diameters of 9.4 and 10.6 nm, respectively. Although the smaller values of the average pore diameters obtained for the composites in comparison with the corresponding value of the TiO_2 aerogel are not surprising at all, the cause for the diminution of their BET area as compared to the unloaded aerogel is not so obvious. An explanation could be the fact that the noble metal particles or their aggregates obstruct part of the TiO_2 aerogel pores.

The photocatalytic tests performed with visible light (by filtering out the UV component) revealed similar photodegradation behavior for both samples **A** and **B**. In this case, the photodegradation rate constants were multiplied by a factor representing the ratio between the incident photon flux for the used UV–vis (2.26×10^{-6} Einstein min^{-1}) and the visible radiation (3.23×10^{-7} Einstein min^{-1}). Very promising results were obtained for both composites, the photodegradation rate values being very similar each other and comparable with those recorded when UV–vis radiation source was employed (see Table 1). However, one notes the remarkable photocatalytic performances of the composite sample with Ag nanoparticles under visible excitation light after the normalizing procedure was applied. In order to get further insights gap energies (E_g) were calculated from diffuse reflectance spectra (see Fig. 3). Thus, E_g values of 3.06 and 2.92 eV were obtained for the composites with Au and Ag, respectively, while for TiO_2 aerogel sample the E_g value was found to be of 3 eV. A possible explanation for the differences observed between the E_g values of the unloaded and the noble metal loaded TiO_2 aerogels is the existence of the noble metal–semiconductor contact. Its presence could lead to a change of the composites electronic structure *via* plasmon-induced charge separation, especially on the charge layer located on the TiO_2 grains surfaces from the close vicinity of the noble metal particle [18]. It is well-known that collective oscillations of electrons are induced on the Au and Ag nanoparticle surface by incident light. In the Au–TiO_2 and Ag–TiO_2 interfacial region, the oscillating electrons may be influenced by the electric

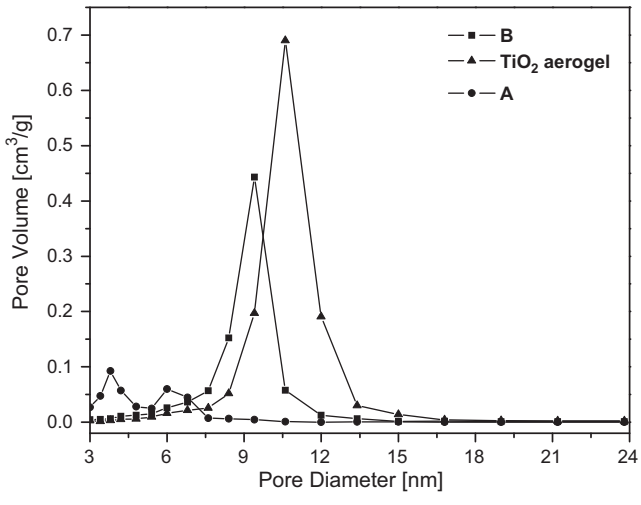

Fig. 2. Pore size distribution of the synthesized porous samples as indicated.

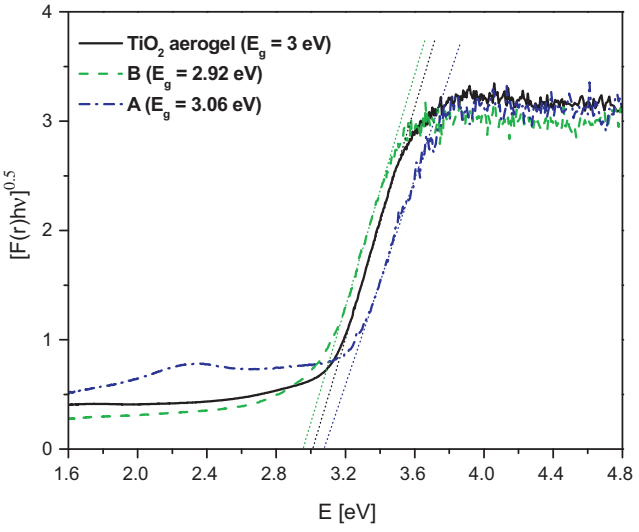

Fig. 3. Diffuse reflectance spectra of the synthesized porous samples as indicated.

field of the existent charge layer causing the transport of electrons to TiO_2 particles. The above-mentioned change may determine in consequence, the modification of the electronic structure in such a way that the absorption spectrum shifts to the visible region. The structural changes induced by the contact between noble metal and TiO_2 particles, especially during supercritical drying process, could certainly represent an additional cause for the appearance of different E_g values. However, for a better understanding of the interfacial energetic behavior of such a complex system, a more simplified semiconductor–noble metal contact must be designed and rigorously evaluated. One should also mention that, in such heterogeneous systems, a transfer of electrons from TiO_2 towards Au nanoparticles concurrently occurs, as a result of Fermi-level equilibration established between the systems [7,18].

The different E_g values obtained when Ag and, respectively, Au nanoparticles are incorporated into TiO_2 aerogel network are most probably due to the plasmon absorption band of the metal nanoparticles. Thus, in the case of the Ag nanoparticles, the band maximum is usually located around 420 nm (2.95 eV), and certainly contributes to the signal recorded and used for E_g calculation, while in the case of Au nanoparticles, the maximum of the plasmon absorption band is situated at ~520 nm, and can be observed around 2.38 eV (~520 nm) in the spectrum illustrated in Fig. 3.

Nevertheless, besides BET surface area, the photocatalytic performances of the porous materials are generally influenced by morphological and structural parameters such as: particles mean size, particle size distribution, and structure type. Therefore, several complementary investigation techniques have been further employed to reveal the morpho-structural features of the composites.

TEM investigations of the samples revealed the existence of almost spherical noble metal nanoparticles, on one hand, and the presence of a more intense aggregation process of the Ag nanoparticles (10–24 nm) in comparison with the Au ones (10–24 nm), on the other hand (Fig. 4). Having in view the small amount of noble metal one can infer that a better dispersion of Au nanoparticles inside the porous titania network exists in comparison with that of the Ag nanoparticles. This behavior was observed from TEM images recorded from various areas of both composites as can be seen from selected pictures presented in the left side insets of Fig. 4. The existence of Au aggregates of smaller dimension in comparison with those of Ag and the better dispersion of Au nanoparticles inside the porous TiO_2 structure contributes to a better understanding of the pore distribution results. Thus, a larger amount of Au nanoparticles than Ag ones are expected to be present inside the pores. This lead to the decreasing of the average value of the pore distribution for composite **A** in comparison with that obtained for composite **B** and TiO_2 aerogel. An amount of crystallized noble metal particles dispersed into the TiO_2 matrix was found from TEM investigations for both composite samples (see fringes from the right side insets of Fig. 4). The dispersion and crystallinity of metallic Au/Ag particles are key factors which undoubtedly influence the interfacial charge transfer between TiO_2 and noble metal particles as well as the photocatalytic properties. On the other hand, every property of semiconducting photocatalysts, e.g. optical properties, dielectric constant, mechanism of diffusion etc., is size dependent [37]. From TEM images analysis it was found that the TiO_2 particles size is in the range between 5 and 15 nm for both composites. The mean size values of the TiO_2 anatase and brookite crystallites from both samples were also determined from XRD data and were found to be of about 10 nm. These values are extremely close to the optimal reported size (~10 nm) that provided the maximum photocatalytic efficiency [1].

XRD measurements of the as-prepared composites also indicate the formation of a major amount of the TiO_2 anatase (about 70%) phase and brookite (about 30%) secondary phase in the composite

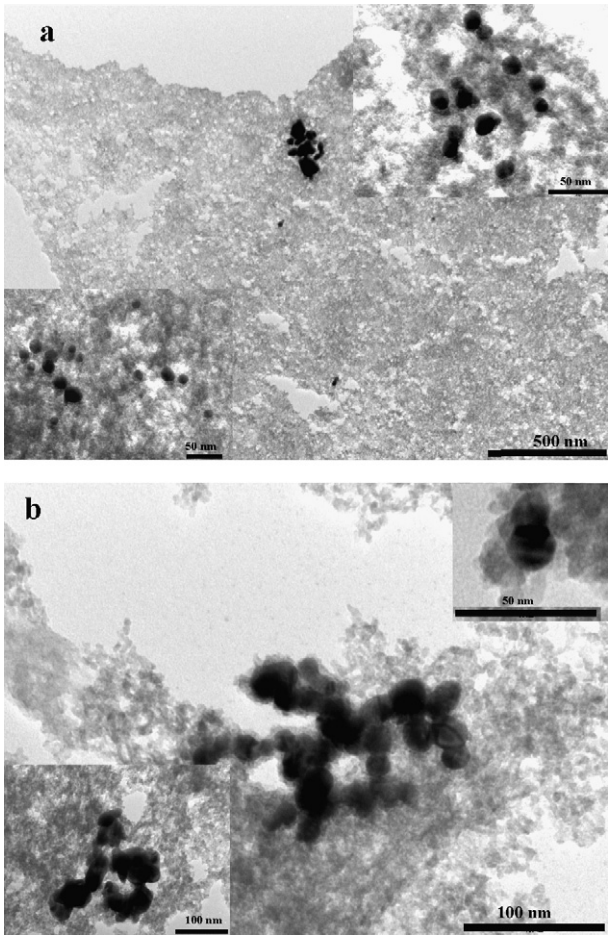

Fig. 4. TEM images of the samples A (a) and B (b). The right side insets show the presence of fringes that indicate the crystalline character for some of Au and Ag nanoparticles. The better dispersion of the Au nanoparticles in comparison with those of Ag is exemplified by the left side insets.

A (Fig. 5c), whereas in the sample **B** a reduced amount of weakly crystallized anatase phase ~15% was found (Fig. 5b) (as shown by the characteristic line intensities in the range of 35–60°). The presence of small amounts of brookite phase is not precluded. No crystalline structure was evidenced after analyzing the TiO_2 aerogel diffractogram (Fig. 5a). These results are confirmed by those of the Raman spectra analysis (see Fig. 6). Thus, in the spectrum of composite **B**, but especially in that of the sample **A**, the signature of both anatase and brookite TiO_2 crystalline phases can be seen around 160 and 636 cm^{-1}. The most intense Raman bands of the TiO_2 anatase and brookite single crystals appears around 144 and 639 cm^{-1}, and around 153, 250 and 636 cm^{-1}, respectively [38–41]. Their presence can be seen in the Raman spectra of the investigated composites as convoluted signals around 160 and 636 cm^{-1}. A few differences between the Raman spectra of the composites and that of the unloaded TiO_2 aerogel can be observed in this spectral range and are due to the non-crystalline nature of the free-noble metal sample that structure is built up from distorted TiO_6 octahedra [38–41].

The excellent and good dispersion of the Au and respectively, Ag colloids inside the aerogel matrix of the composites ensures the efficient contacts between TiO_2 and noble metal nanoparticles and consequently, the improvement of the photocatalytic activity for the UV spectral domain, on the one side, and the extending of the absorption in the visible range, on the other side. A comparison of the photodegradation data determined for the as-prepared composites with those obtained for the commercial Degussa P-25

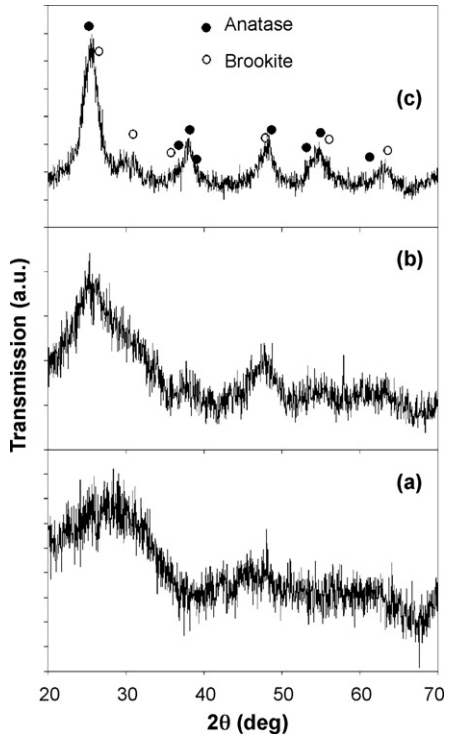

Fig. 5. XRD diffractograms of the TiO_2 aerogel (a) and composites B (b) and A (c).

($k_{app} = 2.5 \times 10^{-3}$ min^{-1}), when a UV–vis radiation source was used, reveals an improvement of the photocatalytic performances by a factor of 12.5 for the sample **A**, and 5.3 for the composite **B**. The better dispersion of the Au nanoparticles inside the titania network in comparison with that exhibited by the Ag nanoparticles, and consequently, the higher number of noble metal-TiO_2 contacts is most probably the main reason that different types of TiO_2 crystalline phase build up the composites **A** and **B** structure.

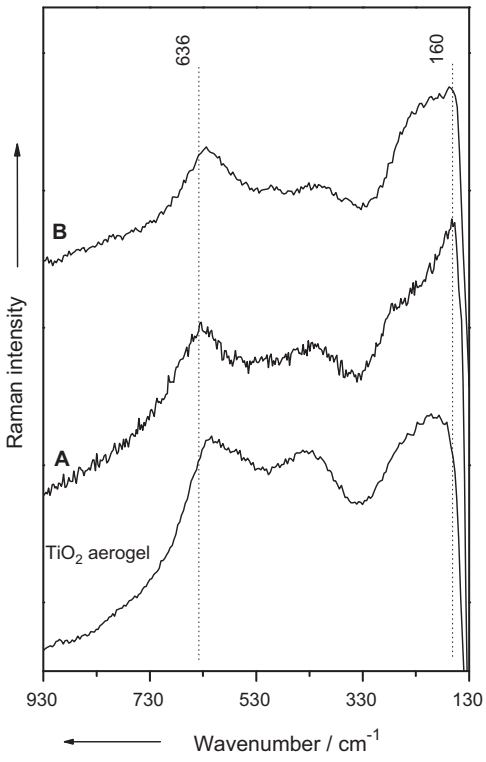

Fig. 6. Raman spectra of the synthesized porous composites as indicated.

In order to understand more about the photodegradation capacity of the synthesized porous samples, their apparent rate constants per surface unit were evaluated and compared with the corresponding values obtained for the unloaded TiO_2 aerogel and the commercial product. Having in view that the size of the crystallites or grains is almost the same, and assuming that the network defects, the structure type or other morpho-structural parameters do not drastically influence the photocatalytic performances, this approach can offer valuable information concerning the importance of the noble metal presence inside the TiO_2 porous network. Thus, it was found that for sample **A** the photodegradation rate of the test molecule on the surface unit (0.093 min^{-1}/m^2) is almost ten times faster than for TiO_2 aerogel (0.01 min^{-1}/m^2) and two times faster than for Degussa P-25 (0.05 min^{-1}/m^2), while in the case of the composite **B** this rate (0.031 min^{-1}/m^2) is three times faster than for TiO_2 aerogel and almost two times slower than for Degussa P-25. Although from this analysis it seems that the composite **B** has a fragile potential in photocatalytic experiments, one must point out its potential for experiments with visible excitation. One can observe the appearance of a considerable enhancement when comparing the data obtained for the unloaded TiO_2 aerogel with those for Au loaded TiO_2 sample. To the best of our knowledge up to now, the effect of the Ag or Au nanoparticle presence inside of a porous structure has not been quantitatively evaluated from the photocatalytic performances perspective. Therefore, one can conclude that, besides the type of the TiO_2 and Au structure that build up the composite structure, an important role for this considerable improvement is played by the existence of the contact between Au and TiO_2 nanoparticles.

In addition to the use of TiO_2 for photocatalytic destruction of water pollutants, the capture of a large amount of sulphates, chlorates, amino and hydroxyl containing contaminants by their adsorption on the noble metal surfaces would certainly contribute to the improvement of the water cleaning process. The porous character of the synthesized composites makes possible the diffusion of pollutant molecules through their three-dimensional network and consequently, their quick detection by taking the benefit of the Raman signal enhancement. Some selected spectra recorded on the composites after their immersion into pollutant aqueous solutions are displayed in Fig. 7 together with the Raman spectra of the free species. A close analysis of the spectra reveals, besides the characteristic bands of TiO_2 (denoted by stars), several fingerprint bands of the contaminants that appear shifted with several wavenumbers relative to their corresponding Raman bands. Thus, in the spectra of composites immersed in thioacetamide solution (Fig. 7a) only the fingerprint band around 715 cm^{-1}, due to the CS stretching vibrations, is clearly observed, while in those of the composites maintained in acrylamide solution (Fig. 7b), the bands around 1630 and 1450 cm^{-1}, given by CC and CN stretching vibrations, and that around 1285 cm^{-1}, attributed to the CH_2 deformation vibration, are observed [42]. The bands present in the spectra of composites immersed in rhodamine 6G (R-6G) solution (Fig. 7c) around 1585 cm^{-1} are given by stretching vibrations of CC from phenyl rings, while those around 1375 cm^{-1} are due to the CC and CN stretching vibrations [43,31]. The distinguished band located at 1170 cm^{-1} in the SERS spectra of composites maintained in R-6G solution (Fig. 7c) is assigned to CH bending vibrations [43,31]. In the spectra of all composites immersed in crystal violet (CV) solution (Fig. 7d) one can see the bands around 1625 cm^{-1}, due to the stretching vibrations of CC from phenyl rings, and those around 1380 and 1175 cm^{-1}, attributed to the CN stretching and CH bending vibrations, respectively [43,31]. The shifts of the SERS bands as compared to the corresponding Raman bands together with the quenching of the fluorescence, especially for the dye molecules,

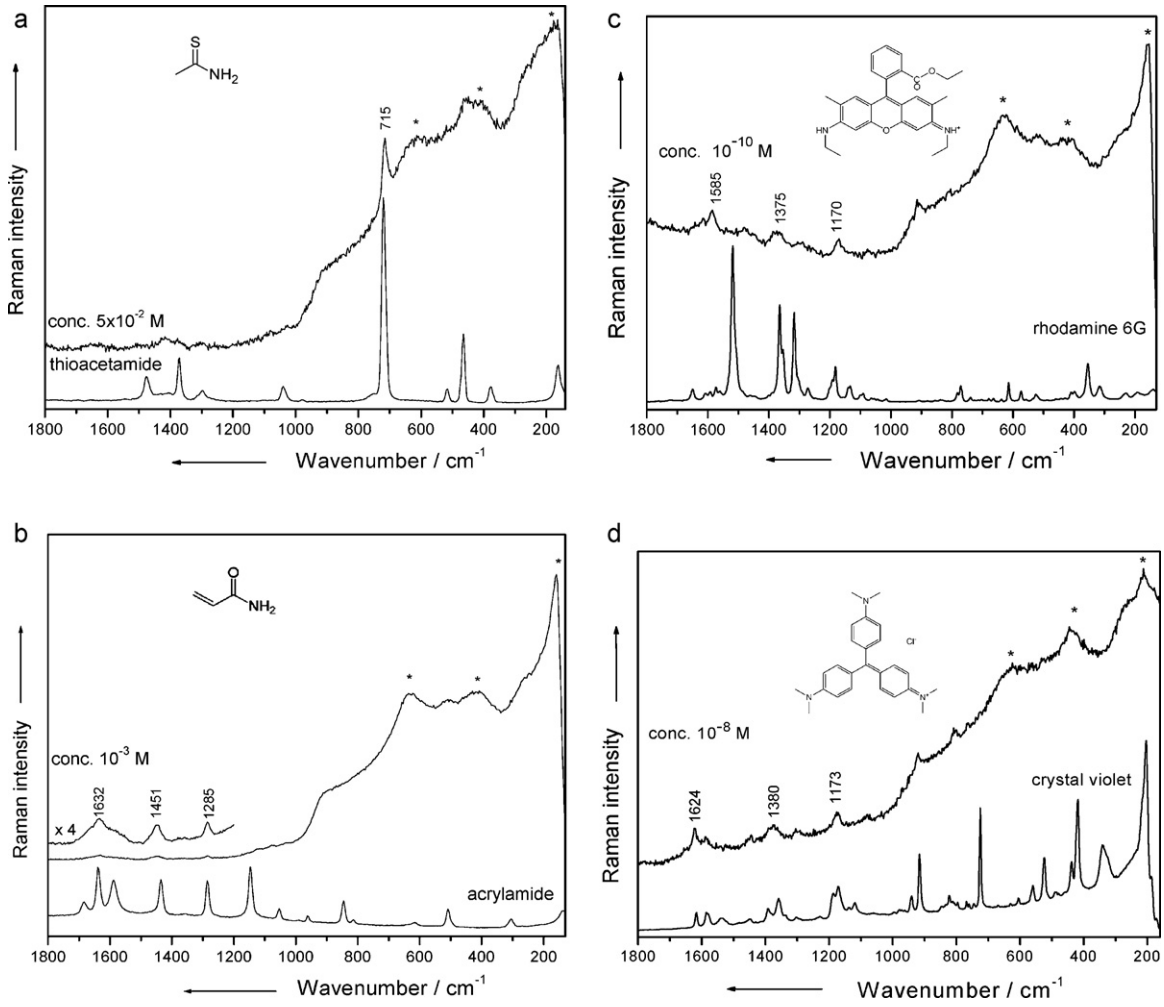

Fig. 7. Raman and selected SERS spectra of different pollutants adsorbed on porous composite **A**, (a) and (d), and on porous composite **B**, (b) and (c). The pollutants type and their concentrations are also indicated. The characteristic bands of TiO_2 are denoted by stars.

account for the pollutant adsorption. The detection sensitivity of both composites was established using for each pollutant molecule solutions of various, but well-established concentrations, and different detection limits were obtained depending on the composite and molecule type. Thus, the detection limit of the thioacetamide compound was found to be of 10^{-3} M, when composite **A** was used, while the smallest detectable concentration of the acrylamide molecule was found to be of 10^{-4} M, when the composite **B** was employed. In the case of dye molecules, the detection limits were found to be 5×10^{-6} M (R-6G, composite **A**) and 10^{-6} M (CV, composite **B**). In certain circumstances, i.e. the electronic absorption of the free molecule coincides or is in close vicinity of the excitation laser line, the detection limit could be improved with several orders of magnitude by recording a resonant SERS signal. In our experiments, CV and R-6G molecules having electronic absorption maxima located at 590 and 524 nm, respectively [43], were tested. In the case of CV molecules adsorbed on Au nanoparticles surface, Raman fingerprints were observed for concentrations of 10^{-8} M, when the 633 nm laser line was employed for excitation (Fig. 7d), while for R-6G molecules adsorbed on Ag nanoparticles surface the detection limit was found to be of 10^{-10} M, when the 532 nm laser line was used (Fig. 7c). It is worth mentioning that similar SERS spectra were recorded from different points inside the samples by focusing several tens of microns. Comparable results were previously found when porous silica matrix–noble metal nanoparticles were employed as a SERS substrate, a limit concentration of 10^{-5} M of dye molecules being detected under resonant excitation [44]. One should emphasize that, in comparison to the SERS performances revealed by the composites analyzed in our previously reported study [31], where the lowest detectable concentrations were found to be of 5×10^{-2} M (thioacetamide) and in the range between 10^{-5} and 10^{-7} M for dye molecules off and under resonant excitation, the samples obtained in the present work exhibit detection sensitivity with at least one order of magnitude higher.

The SERS detection of contaminants with the help of such three dimensional porous systems can open up new perspectives in developing novel SERS based sensors nano-devices. For the analytical applications directed to detect by SERS pollutants from real environments, a well-established selectivity of the adsorbed molecule is the first important requirement. This can be achieved only by creating a SERS database for various pollutants, that fingerprints must be permanently compared with the recorded data. For example, because CS or CN stretching vibrations give SERS bands in a narrow spectral range, their use for such purposes does not represent a complicated task, especially when the water samples under investigations are expected to be polluted with a certain pollutant type.

One of the most important benefits taken from the synthesis of such porous composites by the sol–gel process is the encapsulation of the noble metal particles into the TiO_2 matrix that makes them much more stable in time than the colloids in liquid media [29] and, additionally, avoids their possible contamination. The concen-

tration and the size of the noble metal colloids used to the porous composites synthesis could also influence their functionality. These aspects together with the obtaining of thin porous films based on TiO_2 and Au/Ag nanoparticles are topics already under investigation in our laboratories.

4. Conclusions

In this study we highlight the synthesis of composites based on TiO_2 aerogels and Au and, respectively Ag colloidal particles capable not only to efficiently decontaminate the water (*via* photocatalysis), but also to detect low concentrations of pollutants from water (*via* SERS technique). Improvements (even better than one order of magnitude) of the apparent photodegradation rate constants were obtained, when synthesized composites were employed, in comparison with the results obtained, when commercial Degussa P-25 was used. The ability of noble metal nanoparticles to influence the photocatalytic performances by their presence in the close vicinity of the TiO_2 nanoparticles was evaluated by expressing the photodegradation rate constants to the BET surface unity. Excellent results were obtained for composites based on TiO_2 aerogel and Au nanoparticles. The great potential of the synthesized porous samples for photocatalytic experiments with visible light was also demonstrated. The lowest detectable concentrations of test pollutant molecules adsorbed on the noble metal nanoparticles surface were assessed by SERS and, were found to depend on the composite and pollutant species type. The great detection performances of the porous composites, especially of those containing Ag, recommend them to be used in novel SERS based sensor devices. Thus, when Au containing composites were employed, the detection limits were found to be of 10^{-3} M for thioacetamine and 5×10^{-6} and 10^{-8} M for dye molecule, off and under resonant excitation, respectively, while in the case of Ag containing samples these were found to be of 10^{-4} M for acrylamide and 10^{-6} and 10^{-10} M for dye species, off and under resonant excitation, respectively.

Acknowledgements

This work was supported by CNCSIS-UEFISCSU, project number PN II-RU_TE 81/2010. We gratefully acknowledge Dr. A.M. Vlaicu and Dr. M. Feder for their help with UV–vis and XRD measurements.

References

[1] D. Beydoun, R. Amal, G. Low, S. McEvoy, J. Nanopart. Res. 1 (1999) 439–705.
[2] H. Choi, M.G. Antoniou, M. Pelaez, A.A. De la Cruz, J.A. Shoemaker, D.D. Dionysiou, Environ. Sci. Technol. 41 (2007) 7530–7535.
[3] S. Malato, J. Blanco, J. Cáceres, A.R. Fernández-Alba, A. Agüera, A. Rodríguez, Catal. Today 76 (2002) 209–220.
[4] S. Sakthivel, M.V. Shankar, M. Palanichamy, B. Arabindoo, D.W. Bahnemann, V. Murugesan, Water Res. 38 (2004) 3001–3008.
[5] P.V. Kamat, J. Phys. Chem. B 106 (32) (2002) 7729–7744.
[6] P.D. Cozzoli, E. Fanizza, R. Comparelli, M.L. Curri, A. Agostano, J. Phys. Chem. B 108 (2004) 9623–9630.
[7] V. Subramanian, E.E. Wolf, P.V. Kamat, J. Am. Chem. Soc. 126 (2004) 4943–4950.
[8] C. Burda, Y. Lou, X. Chen, C.S. Samia Anna, J. Stout, J.L. Gole, Nano Lett. 3 (2003) 1049–1051.
[9] P.V. Kamat, M. Flumiani, A. Dawson, Colloids Surf. A: Physicochem. Eng. Aspects 202 (2002) 269–279.
[10] A. Orlov, D.A. Jefferesson, M. Tirkov, R.M. Lambert, Catal. Commun. 8 (2007) 821–824.
[11] Y. Denkwitz, J. Geserick, U. Hörmann, V. Plzak, U. Kaiser, N. Hüsing, R.J. Behm, Catal. Lett. 119 (3–4) (2007) 199–208.
[12] B. Xin, L. Jing, Z. Ren, B. Wang, H.G. Fu, J. Phys. Chem. B 109 (2005) 2805–2809.
[13] J.J. Pietron, R.M. Stroud, D.R. Rolison, Nano Lett. 2 (5) (2002) 545–549.
[14] V. Subramanian, E.E. Wolf, P.V. Kamat, Langmuir 19 (2003) 469–474.
[15] N. Chandrasekharan, P.V. Kamat, J. Phys. Chem. B 104 (2000) 10851–10857.
[16] A. Dawson, P.V. Kamat, J. Phys. Chem. B 105 (2001) 960–966.
[17] P.D. Cozzoli, M.L. Curri, A. Agostiano, Chem. Commun. 25 (2005) 3186–3188.
[18] Y. Tian, T. Tatsuma, Chem. Commun. (2004) 1810–1811.
[19] M. Valden, X. Lai, D.W. Goodman, Science 281 (1998) 1647–1650.
[20] G.R. Bamwenda, S. Tsubota, T. Nakamura, M. Haruta, Catal. Lett. 44 (1997) 83–87.
[21] N. Hüsing, U. Schubert, Chem. Int. Ed. 37 (1998) 22–47.
[22] G. Dagan, M. Tomkiewicz, J. Phys. Chem. 97 (1993) 12651–12655.
[23] M. Baia, L. Baia, J. Popp, S. Astilean, Appl. Phys. Lett. 88 (2006) 1431211–1431213.
[24] L. Baia, M. Baia, J. Popp, S. Astilean, J. Phys. Chem. B 110 (2006) 23982–23986.
[25] S. Nie, S.R. Emory, Science 275 (1997) 1102–1106.
[26] M.A. De Jesús, K.S. Giesfeldt, M.J. Sepaniak, J. Raman Spectrosc. 35 (2004) 895–904.
[27] E.A.F. Carrasco, M. Campos-Vallette, P. Leyton, G.F. Diaz, R.E. Clavijo, J. Phys. Chem. A 107 (2003) 9611–9619.
[28] T. Vo-Dinh, Sens. Actuators B 29 (1995) 183–189.
[29] G.A. Baker, D.S. Moor, Anal. Bioanal. Chem. 382 (2005) 1751–1770.
[30] H. Schmidt, N.B. Ha, J. Pfannkuche, H. Amann, H.D. Kronfeldt, G. Kowalewska, Mar. Pollut. Bull. 49 (2004) 229–234.
[31] M. Baia, V. Danciu, V. Cosoveanu, L. Baia, Vib. Spectrosc. 48 (2008) 206–209.
[32] C.D. Keating, M.D. Musick, M.H. Keefe, M.J. Natan, J. Chem. Educ. 76 (1999) 949–955.
[33] P.C. Lee, D. Meisel, J. Phys. Chem. 86 (1982) 3391–3395.
[34] M. Tomkiewicz, Catal. Today 58 (2000) 115–123.
[35] T. Rajh, L.X. Chen, K. Lukas, T. Liu, M.C. Thurnauer, D.M. Tiede, J. Phys. Chem. B 106 (2002) 10543–10552.
[36] L. de la Garza, Z.V. Saponjic, N.M. Dimitrijevic, M.C. Thurnauer, T. Rajh, J. Phys. Chem. B 110 (2006) 680–686.
[37] S. Kelly, F.H. Pollak, M. Tomkiewicz, J. Phys. Chem. B 101 (1997) 2730–2734.
[38] Y.H. Zhang, C.K. Chan, J.F. Porter, W. Guo, J. Mater. Res. 13 (1998) 2602–2609.
[39] L. Baia, A. Peter, V. Cosoveanu, E. Indrea, M. Baia, J. Popp, V. Danciu, Thin Solid Films 511–512 (2006) 512–516.
[40] L. Baia, M. Baia, A. Peter, V. Cosoveanu, V. Danciu, J. Optoelectr. Adv. Mater. 9 (3) (2007) 668–671.
[41] V. Danciu, L. Baia, V. Cosoveanu, M. Baia, F. Vasiliu, L. Diamandescu, C.M. Teodorescu, M. Feder, J. Popp, Optoelectr. Adv. Mater.-Rapid Commun 2 (2) (2008) 76–80.
[42] A.S.R. Duarte, A.M. Amorim da Costa, A.M. Amado, J. Mol. Struct.: TheoChem 723 (1–3) (2005) 63–68.
[43] A. Kudelski, Chem. Phys. Lett. 414 (2005) 271–275.
[44] R. Gilbert, Improved SERRS Substrate, WO/2007/110614.